Optical Properties of Anisotropic Core−Shell Pyramidal Particles†

Christina M. Sweeney,‡ Warefta Hasan,‡ Colleen L. Nehl,‡ and Teri W. Odom*,‡,§

Department of Chemistry, Department of Materials Science and Engineering, Northwestern University, 2145 Sheridan Road, Evanston, Illinois 60208-3113

Received: December 9, 2008; Revised Manuscript Received: January 26, 2009

This paper describes an approach to fabricate anisotropic core−shell particles by assembling dielectric beads within fabricated noble metal pyramidal structures. Particles with gold (Au) shells and different dielectric cores were generated, and their optical properties were characterized by single particle spectroscopy. Because of their unique geometry, these particles exhibit multiple plasmon resonances from visible to near-IR wavelengths.

Core−shell particles (in particular, spherical particles with dielectric cores surrounded by metallic shells) are interesting because of their highly tunable localized surface plasmon resonances.[1−6] These resonances can be shifted hundreds of nanometers simply by changing the thickness of the shell layer or by changing the bulk refractive index (n) of the surrounding environment.[7] Particles with dielectric cores have proven especially useful in biomedical applications because they enable targeted cell death as a result of photothermal heating at near-infrared wavelengths (650−900 nm).[3,8−10] Core−shell particles (diameters, $d > 70$ nm) with varying compositions have been synthesized by first seeding the core with Au nanoparticles, followed by the reduction of metal ions from solution onto the dielectric bead to form the shell. For example, particles with silica (SiO_2) or polystyrene (PS) cores and Ag or Au shells have been synthesized with controllable shell thicknesses between 5 and 20 nm.[2,3,5,6]

The synthesis of new types of core−shell particles requires either a modification of the core to promote metal seeding or the development of metal reduction strategies that can fully encapsulate the core. Fabrication strategies provide an approach to circumvent these chemical modification schemes, although most reports have only produced beads whose top surfaces were coated with metal. For example, e-beam deposition of Au onto SiO_2 beads followed by chemical etching of the SiO_2 resulted in Au "half-shell" particles that could be assembled into arrays and functionalized to be superhydrophobic.[11] Similarly, modulated optical nanoprobes, which can be used as solution-based fluorescence tags, were fabricated by deposition of Au onto fluorescent PS particles.[12]

Here we describe a method to fabricate pyramidal core−shell particles by first assembling beads into pyramidal shells and then encapsulating the beads by e-beam deposition to form the top shells. Our strategy enables the creation of core−shell nanoparticles with complex shapes, controllable dimensions, and flexible compositions with optical properties tunable at NIR wavelengths. Figure 1A outlines the fabrication scheme used to generate our core−shell particles. PEEL (**p**hase-shifting photolithography (PSP), **e**tching, **e**-beam, and **l**ift-off) was used

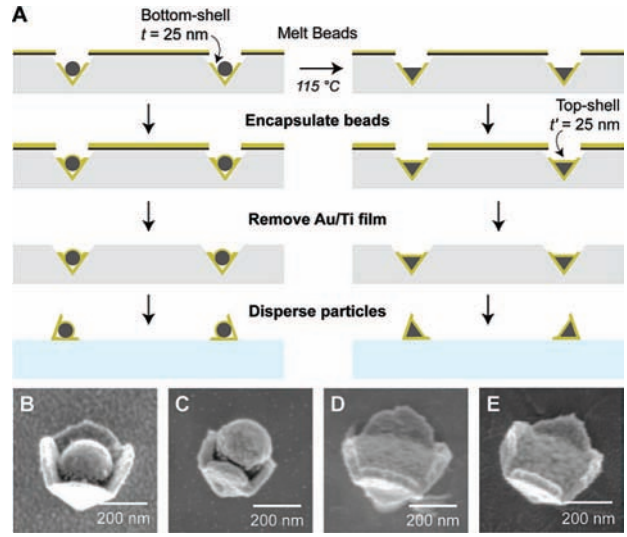

Figure 1. Core−shell particle assembly strategy. (A) Assembly of PS or SiO_2 beads into pyramidal bottom shells, encapsulated with top shells, and then released to form pyramidal core−shell particles. (B, C) SEM images of Au−PS−Au particles with separated bottom and top shells because of swelling by the PS beads under e-beam deposition. (D, E) SEM images of Au−PS_{melt}−Au particles with flat dielectric surfaces covered by a top shell.

to fabricate the bottom pyramidal shell.[13] In previous work, Cr was used as the material for the etch and deposition mask;[13] in this work, Ti was used because lift-off was easier. In brief, a Ti film perforated with 350-nm holes served as an etch mask through which the underlying Si (100) was anisotropically etched as well as a deposition mask through which Au (thickness, $t = 25$ nm) was deposited to form pyramidal shells. For all the core−shell pyramidal particles, t was kept constant.

We assembled the cores of our particles, either PS beads ($d = 202$ nm, $n = 1.59$; Polysciences, Warrington, PA) or SiO_2 beads ($d = 225$ nm, $n = 1.46$), into the bottom shells by first drop-casting a solution of beads onto the template and then dragging a slab of PDMS (Dow Corning, Germantown, WI) across the surface so that the beads would settle into the pyramidal pits in a manner similar to gravure and high-resolution particle printing.[14] We also assembled multiple, smaller-diameter beads into individual shells, but to fabricate core−shell particles with a single bead with over 90% surface coverage, we chose beads with diameters of ∼200 nm to maintain a size ratio of

† Part of the "George C. Schatz Festschrift".

* To whom correspondence should be addressed. E-mail: todom@northwestern.edu.

‡ Department of Chemistry.

§ Department of Materials Science and Engineering.

10.1021/jp810837u CCC: $40.75
Published on Web 03/16/2009

1.7 with the hole in the Ti film.[15] Core−shell pyramidal particles were also fabricated with melted PS cores (PS_{melt}) by heating the assembled beads in the substrate to 388 K in a muffle furnace for 15 min. Heating the PS above its glass transition temperature, T_g (373 K), allowed the PS to flow and fill the cavity of the pyramidal shell.

Pyramidal core−shell particles were completed by e-beam deposition of Au to form the top shells (thickness $t' = 25$ nm). For unmelted PS bead structures, we situated the sample on a tilted stage ($\theta = 15°$) that rotated at 800 rpm. The tilted stage allowed the interface between the bead and the inner surface of the bottom pyramidal shell to be coated with metal. PS beads would often swell because of elevated temperatures during the deposition, however, which resulted in a small gap between the top shell and the inner surface of the bottom shell (Figure 1B, C). For melted PS cores, the encapsulation was carried out by line-of-site deposition: because the top surface of the PS core was flat, there was no shadowing at the interface between the bottom shell and the core (Figure 1D, E). The Au/Ti film was then removed by soaking the substrates for 5−10 s in Ti etchant (Transene, Danvers, MA), which dissolved the Ti mask and released the Au film to leave encapsulated, pyramidal core−shell particles. The particles were removed from the Si template by etching in gaseous XeF_2 (XACTIX, Inc. Xetch e1 series, Xenon Difluoride Etcher: Xactix, Pittsburgh, PA) and then sonicating in water.

Single particle, dark-field (DF) spectroscopy was used to characterize the optical properties of the pyramidal core−shell particles. Scattered light from the particles was collected with a variable numerical aperture objective (100×, NA = 0.5) under DF illumination using an inverted optical microscope (Nikon TE2000-U, Melville, NY). Spectra were analyzed using a spectrometer (Jovin-Yvon TRIAX 550 and CCD, Jovin-Yvon Symphony Jovin-Yvon, Edison, NJ) equipped with a LN_2 cooled imaging CCD detector (Jovin-Yvon Symphony). The dielectric environment surrounding the particles was changed using immersion oils (Cargille, Cedar Grove, NJ) with different refractive indices (n = 1.29, 1.40, 1.51, 1.60). To correlate scattering spectra with SEM images, core−shell particles were dispersed onto ITO-coated (Delta Technologies, Stillwater, MN) glass substrates (n_{ITO} = 1.8) patterned with markers. As discussed in previous work, Au pyramidal shells (the bottom shell of our core−shell particles) exhibit orientation-dependent properties.[16−18] When the tips point away from the surface (tip-up), the structures have higher intensity spectral features at lower wavelengths (550−750 nm). In contrast, when the tips touch the surface (tip-down), the structures have spectral features of comparable intensity at both low and high wavelengths (550−950 nm). Because pyramidal core−shell particles favor a tip-down configuration, all particles were characterized in the tip-down orientation.

Figure 2 highlights the differences between two types of polystyrene core−shell particles: Au−PS−Au and $Au-PS_{melt}-Au$. Au−PS−Au particles exhibited scattering peaks at 640 and 900 nm, with the former being less intense than the latter. In contrast, the spectra of the $Au-PS_{melt}-Au$ particles had sharper features and were composed of a shoulder at 600 nm, peaks at 665 and 770 nm, and a higher intensity peak at 875 nm. The blue resonances of both particles were slightly less intense than the red ones, and the long- and short-wavelength resonances had similar peak positions. Because the dielectric materials were identical, differences in the number of spectral features as well as their sharpness can be attributed to either the change in shape of the dielectric, the gap between

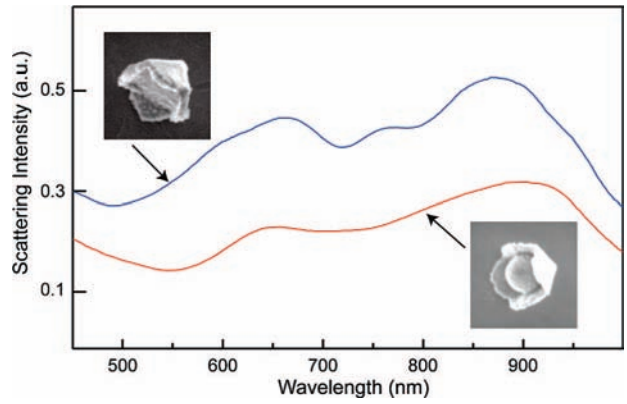

Figure 2. Comparison of PS core−shell particles with different shapes. Single-particle spectroscopy comparing Au−PS−Au (blue) and $Au-PS_{melt}-Au$ (red) pyramidal core−shell particles in $n = 1.51$. SEM images are 600 × 600 nm.

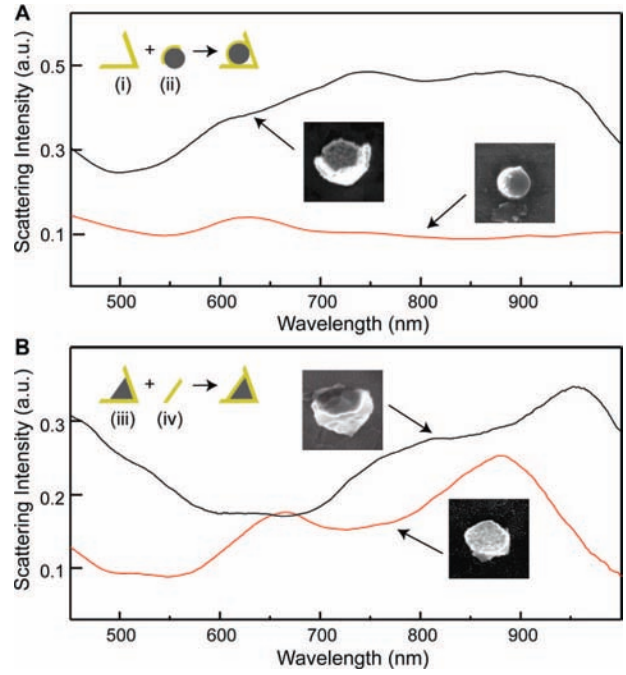

Figure 3. Comparison of core−shell structural components. (A) Single-particle spectra of core−shell structural components for Au−PS−Au: (i) Au bottom shells and (ii) spherical PS beads with Au top shell. (B) Single-particle spectra of core−shell structural components for $Au-PS_{melt}-Au$: (iii) Au bottom shell with melted PS beads, and (iv) a flat Au top shell. $n = 1.51$ for all measurements. SEM images are 600 × 600 nm.

the bottom shell and top shell of the Au−PS−Au particle, or both. To investigate the origin of the differences between the spectra, we analyzed the individual structural components of the pyramidal core−shell particles. This ability to fabricate and characterize separated components is a unique advantage of our fabrication procedure (Figure S1 of the Supporting Information). Figure 3 displays the cartoons and spectra of the four components: (i) Au bottom shell; (ii) spherical PS bead with Au top shell; (iii) Au bottom shell with melted PS; and (iv) flat Au top shell. Structurally, Au−PS−Au particles can be considered as a combination of components i and ii, which is also supported by SEM images that showed that the top shell and bottom pyramidal shells were not physically connected. Note that (i) has upper edges that are thicker than $t = 25$ nm because of the angled deposition through the Ti mask (but without the bead) necessary to mimic the Au−PS−Au particles. Analysis of the

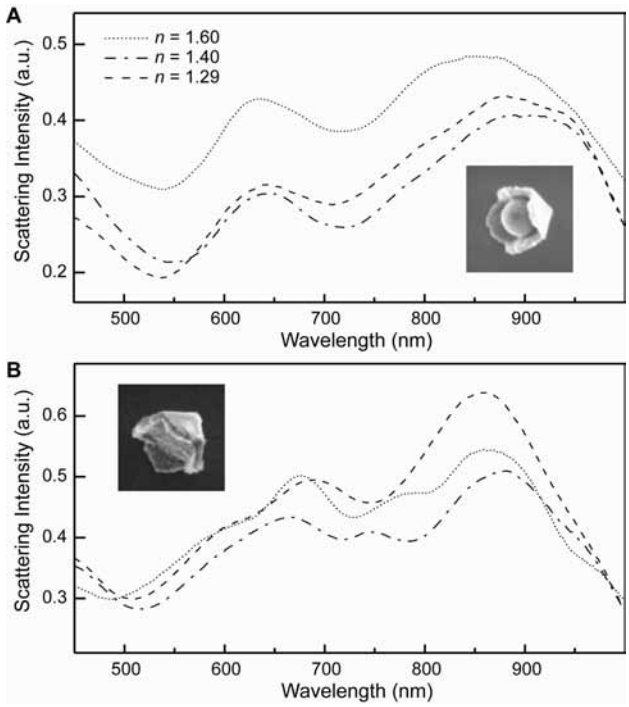

Figure 4. Refractive index investigation of pyramidal core−shell particles. Single particle scattering spectra under different refractive indices (n = 1.29, 1.40, and 1.60) for (A) Au−PS−Au and (B) Au−PS_{melt}−Au particles. SEM images are 600 × 600 nm.

individual parts—(i) with high intensity resonances in the red and (ii) with a single resonance at 625 nm—suggests that the spectra of these components can be combined to generate the plasmon features of the Au−PS−Au particles at nearly the same wavelengths (Figure 3A). Although the resonance at 750 nm is present in component (i), this feature is not observed in the Au−PS−Au spectra, possibly because of either damping effects from interactions between the shell and the bead or small morphological differences in the capping layer from the angled deposition.

Similarly, Au−PS_{melt}−Au core−shell particles can be constructed from components (iii) and (iv); however, in the case of these structures, the two components are connected. Investigation of these components—(iii) with two high intensity resonances in the far-red and (iv) with resonances at 660 and 890 nm—supports the hypothesis that the surface plasmon features of the components can be combined to generate the optical characteristics of the pyramidal core−shell structures (Figure 3B). The resonances of the Au−PS_{melt}−Au particles were blue-shifted relative to its component resonances (Figure S2 of the Supporting Information). We attribute this blue-shift to increased interactions between the top and bottom shells because no shifting was observed for the Au−PS−Au particles (which have separated top and bottom shells).

To investigate how the spectral features of the core−shell pyramidal particles evolved under different dielectric environments, we changed the bulk n (Figure 4). The plasmon resonances of both Au−PS−Au and Au−PS_{melt}−Au particles red-shifted with increasing n with a few notable exceptions: (1) the Au−PS−Au particle resonances blue-shifted under n = 1.60, which may be from index-matching between the oil and the PS; (2) the Au−PS_{melt}−Au resonance at 890 nm shifted blue with increasing n; and (3) the Au−PS_{melt}−Au spectrum in n = 1.29 had only one prominent peak between 600−750 nm, which may be a result of the two short wavelength peaks overlapping

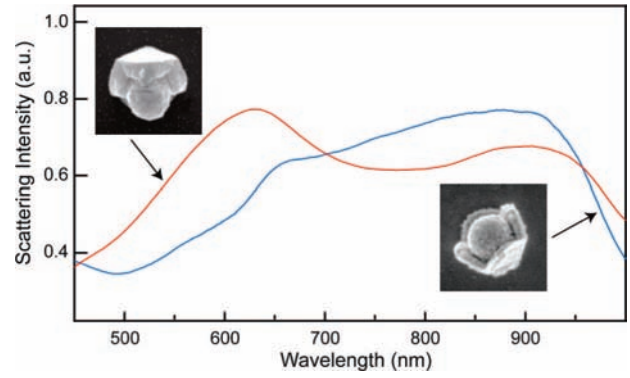

Figure 5. Comparison of SiO_2 cores with different top-shell thicknesses. Single-particle scattering spectra of Au−SiO_2−Au for which t' = 25 nm (blue) and t' = 65 nm (red) in n = 1.51 media. SEM images are 600 × 600 nm.

or as a result of different resonance behavior in lower index media. Notably, the spectral features of the Au−PS_{melt}−Au particles were more sensitive to changes in n.

We investigated further the additive nature of the structural and optical properties of the components to produce pyramidal core−shells by analyzing the individual components (i)−(iv) under different n. Investigation of the optical spectra of the components provides some initial qualitative insight into the origins of the spectral features observed in the core−shell particle. For the case of Au−PS−Au particles (composed of i and ii), the spectra of i displayed similar resonance behavior under n = 1.60 and n = 1.51; however, in n = 1.29, the spectra changed into a broad, strong peak at long wavelengths (Figure S3 of the Supporting Information). The plasmon resonance of (ii) did not shift significantly under different n (Figure S4 of the Supporting Information), and the position was similar to the feature at 640 nm in the Au−PS−Au core−shell spectra. Because the spectral properties of these particles appear to be additive (we do not claim that they are an exact sum because of different local environments), large shifts in peak positions were not observed for Au−PS−Au particles in different dielectric environments because: (1) the red resonance position is most affected by the refractive index inside (i); and (2) the blue resonance is mostly from (ii), which showed only small red-shifts under increased n. For the Au−PS_{melt}−Au particles (composed of (iii) and (iv)), the spectra of iii showed little change in resonance position with n (Figure S5 of the Supporting Information). Significant peak shifts were observed for (iv) under different n, however, and especially under n = 1.29, where an additional resonance appeared in the far-red, and the resonance at 890 nm blue-shifted (Figure S6 of the Supporting Information). Thus, the longer wavelength spectral features of the Au−PS_{melt}−Au core−shell particles seem to be dominated by contributions from (iv).

To demonstrate the flexibility of our fabrication method, we changed the core material to SiO_2 and increased the top-shell thickness. SiO_2 beads were synthesized by the base-catalyzed hydrolysis of tetraethylorthosilicate (Sigma-Aldrich, St. Louis, MO) via the Stöber method.[19] The Au−SiO_2−Au particles (t = 25 nm, t' = 25 or 65 nm) were fabricated using the same assembly and tilted encapsulation method as Au−PS−Au. In the SiO_2 core case, there was no swelling of the bead, and hence, the particles were fully encapsulated. These particles also had spectral features similar to the Au−PS−Au particles with strong resonances at ~600 and 915 nm on a broad background (Figure 5). Although both Au−SiO_2−Au particles had a resonance at 915 nm, the blue resonance for the thicker top-shell particles

shifted to lower wavelengths and became more intense than the red resonance. These changing peak intensities and blue-shifted resonances were similar to observations where the spherical core−shell particles had more shell material on one side than the other.[20]

Au−SiO_2−Au particles ($t' = 25$ nm) were also analyzed under different refractive index environments, where the red resonance shifted to longer wavelengths with increasing n (Figure S7 of the Supporting Information). The intensity and peak position of the resonances are also similar to the Au−PS−Au particle, which suggests that the broadness of the peaks may be attributed in part to the air gap at the tip.

In summary, we have reported a highly controllable method for producing pyramidal core−shell particles with different dielectric cores. The properties can be altered by (1) changing the shape of the dielectric core or (2) increasing the top-shell thickness. Our assembly strategy allows us to investigate how the individual components of the core−shell particles contribute to the optical properties, which enables a detailed understanding of the spectral properties of the particles. With the ability to fabricate anisotropic core−shell particles with virtually any material encapsulated, we anticipate this work will find applications as particles for photothermal therapy, as vectors for the delivery of therapeutics, or as optical scattering tags for biological targets.

Acknowledgment. This work was supported in part by the NSF MRSEC program at Northwestern University (DMR-0520513), the David and Lucile Packard Foundation, and the NIH Director's Pioneer Award (DP1OD003899). This work used the NUANCE and IMSERC Center facilities, which are supported by NSF-MRSEC, NSF-NSEC, and the Keck Foundation.

Supporting Information Available: Spectra of structural components under different n. Fabrication schemes for fabricating core−shell structural components. Spectra of Au−SiO_2−Au particles under different n. This material is available free of charge via the Internet at http://pubs.acs.org.

References and Notes

(1) Halas, N. *MRS Bull.* **2005**, *30*, 362.
(2) Oldenburg, S. J.; Westcott, S. L.; Averitt, R. D.; Halas, N. J. *J. Chem. Phys.* **1999**, *111*, 4729.
(3) Loo, C.; Lin, A.; Hirsch, L.; Lee, M.-H.; Barton, J.; Halas, N.; West, J.; Drezek, R. *Technol. Cancer Res. Treatment* **2004**, *3*, 33.
(4) Oldenburg, S. J.; Averitt, R. D.; Westcott, S. L.; Halas, N. J. *Chem. Phys. Lett.* **1998**, *288*, 243.
(5) Yong, K.-T.; Sahoo, Y.; Swihart, M. T.; Prasad, P. N. *Colloids Surf., A* **2006**, *290*, 89.
(6) Shi, W.; Sahoo, Y.; Swihart, M. T.; Prasad, P. N. *Langmuir* **2005**, *21*, 1610.
(7) Tam, F.; Moran, C.; Halas, N. *J. Phys. Chem. B* **2004**, *108*, 17290.
(8) Weissleder, R. *Nat. Biotechnol.* **2001**, *19*, 316.
(9) Hu, M.; Novo, C.; Funston, A.; Wang, H.; Staleva, H.; Zou, S.; Mulvaney, P.; Xia, Y.; Hartland, G. V. *J. Mater. Chem.* **2008**, *18*, 1949.
(10) Au, L.; Zheng, D.; Zhou, F.; Li, Z.-Y.; Li, X.; Xia, Y. *ACS Nano* **2008**, *2*, 1645.
(11) Love, J. C.; Gates, B. D.; Wolfe, D. B.; Paul, K. E.; Whitesides, G. M. *Nano Lett.* **2002**, *2*, 891.
(12) Behrend, C. J.; Anker, J. N.; McNaughton, B. H.; Brasuel, M.; Philbert, M. A.; Kopelman, R. *J. Phys. Chem. B* **2004**, *108*, 10408.
(13) Henzie, J.; Kwak, E.-S.; Odom, T. W. *Nano Lett.* **2005**, *5*, 1199.
(14) Kraus, T.; Malaquin, L.; Schmid, H.; Riess, W.; Spencer, N. D.; Wolf, H. *Nat. Nano.* **2007**, *2*, 570.
(15) Yin, Y.; Xia, Y. *Adv. Mater.* **2001**, *13*, 267.
(16) Lee, J.; Hasan, W.; Lee, M. H.; Odom, T. W. *Adv. Mater.* **2007**, *19*, 4387.
(17) Shuford, K. L.; Lee, J.; Odom, T. W.; Schatz, G. C. *J. Phys. Chem. C* **2008**, *112*, 6662.
(18) Hasan, W.; Lee, J.; Henzie, J.; Odom, T. W. *J. Phys. Chem. C* **2007**, *111*, 17176.
(19) Stöber, W.; Fink, A.; Bohn, E. *J. Colloid Interface Sci.* **1968**, *26*, 62.
(20) Wang, H.; Wu, Y.; Lassiter, B.; Nehl, C. L.; Hafner, J. H.; Nordlander, P.; Halas, N. J. *Proc. Natl. Acad. Sci.* **2006**, *103*, 10856.

JP810837U